Communications in Physics, Vol. 32, No. 2 (2022), pp. 213-222
DOI: https://doi.org/10.15625/0868-3166/15921

EFFECT OF CU^{2+} DOPANT ON THE FORMATION OF ZINC OXIDE MICROROD FABRICATED BY A HYDROTHERMAL METHOD

LUU THI LAN ANH[1], LE PHUOC SANG[2] AND NGUYEN XUAN SANG[2,†]

[1]*School of Engineering Physics, Hanoi University of Science and Technology, No 1, Dai Co Viet, Hanoi 100000, Vietnam*

[2]*Saigon University, 273 An Duong Vuong, ward 3, district 5,Ho Chi Minh City 700000,Vietnam*

E-mail: [†]sangnguyen@sgu.edu.vn

Received 8 March 2021; *Accepted for publication 4 October 2021*; *Published 18 April 2022*

Abstract. *Reconstruction and stabilization of polar oxide surfaces, such as ZnO, contribute a significant role in photocatalysis, chemical sensing, and optoelectronic applications, however their physical chemistry insight is still a puzzle in the surface science. In this work, the* (0001) *polar surface instability induced by the morphological evolution of hydrothermally synthesized micro-rod ZnO doped with various contents of* Cu^{2+} *ion (1-10 at.%) was investigated. The transformation of micro-rod morphology from the high aspect ratio flower-like shape of the pure ZnO to the hexagonal prism-like shape of the doped ZnO was characterized by the X-ray diffractometry, the scanning electron microscopy and the micro Raman spectroscopy. The chemically active Zn-terminated polar surface in doped samples was less positive charge density which was the main reason to cancel the electrostatic instability for the dominant* $[0001]$ *growing direction. Furthermore, the schematic models of the electron transferring from the conduction band region to the electron trap centre of* Cu^{2+}*, and the Zn-terminated polar surface reconstruction were proposed for the morphological evolution mechanism.*

Keywords: Cu ion dopant; growth models; morphology; hydrothermal; ZnO microstructures.

Classification numbers: 61.72.uj; 61.46.Km.

I. INTRODUCTION

The understanding of oxide surface reconstruction is of interest in surface chemistry and semiconductor technology [1–3]. The anisotropy growth along the $[0001]$ direction in the hexagonal wurtzite zinc oxide (ZnO), the most favorable growth direction of the ZnO, is prominent as a

high polar surface energy in both positive Zn-terminated and negative O-terminated charge planes which are crucial in photocatalysis, light emitting, gas sensor [4–6]. In addition, one-dimensional (1D) ZnO nano/microstructures play important roles as interconnects or functional units in fabricating nanoscale devices [7, 8]. Dopings ZnO with other elements to obtain diluted magnetic semiconductors were reported owing magnetic property that makes promising application in spintronics [9]. Recently, ZnO doped with various transition metal ions has been studied intensively for photocatalytic applications due to the heterogeneous formation between transition ions and the ZnO host lattice which reduced electron-hole recombination rate [10–12]. However, when introducing transition ions into 1D ZnO, the ZnO morphology was shown a dramatic change [13–15]. Sahai *et al.* [13] reported ZnO morphology was changed from rod-like to pyramid-like shape by doped ion Fe due to the ionic size difference between Zn^{2+} and $Fe^{3+/2+}$. The morphology evolution explanation based on the difference of ionic radii was not convinced because there several parameters should be carefully considered such as the high polar energy of the $[0001]$ direction, the interplane distances between positive Zn-terminated and negative O-terminated surfaces, surface charge density, and the electron transferring from conduction band region of the unintentional *n*-type ZnO to dopant centers [2, 16–18]. Other works on the morphology evolution of ZnO doped Cu^{2+} were also reported recently by Kadam [14] and Babikier [15]. In the Babikier's work, the diameter size and crystalline quality of nanorod arrays of ZnO doped Cu^{2+} strongly depended on the precursor of Cu ion sources where the pH value of the starting solution played an important role.

In this work, we report the observation of a morphological evolution from micro-rod to micro-prism of ZnO doped Cu^{2+} fabricated by a simple hydrothermal method in the solution of hexamethylenetetramine (HMTA). Crystalline structure and phase information were characterized by the X-ray diffraction (XRD; X'Pert PRO PANalytical-Phillip, $\lambda = 1.540560$ Å) and the micro-Raman spectroscopy (Renishaw, $\lambda = 633$ nm He-Ne laser as the excitation source). The evolution of ZnO morphology was analyzed by the scanning electron spectroscopy (SEM; JEOL JSM-7600F). Furthermore, the mechanism of morphological evolution of Cu-doped ZnO microrods was proposed in terms of polar surface energy instability and the conduction band electron transferring.

II. EXPERIMENTAL

ZnO microstructures doped with the transition metal ion Cu^{2+} were prepared by a facile one-pot hydrothermal method. All the chemicals were purchased and used without further purification. In order to prepare Cu^{2+} doped in ZnO nanostructure, the synthesis procedure is as follows: 50 mL of 0.1M $Zn(NO_3)_2$ (Merck) was added to distilled water, then HMTA (Xilong) was dissolved in this solution with HMTA : $Zn(NO_3)_2$ molar ratio = 1 : 1 under the magnetic stirring condition. In the synthesis process, $Cu(NO_3)_2$ (Merck) solution was added dropwise to obtain proper molar concentrations of ion Cu^{2+} in ZnO: 1.0, 2.0, 3.0, 4.0, 5.0, and 10 at.% (which were named as C1, C2, C3, C4, C5, and C10, respectively). The resulted solution was stirred in 10 min, then, poured into a Teflon-lined autoclave and hydrothermally heated at 90°C for 6 h. After the hydrothermal process, the autoclave was naturally cooled to room temperature and the precipitate was washed by bi-distilled water until a pH of 7 was reached. Finally, the drying process was applied at 100°C in an oven until a completely dry powder was obtained.

III. RESULTS AND DISCUSSION

III.1. X-ray Diffraction (XRD)

The pure ZnO and ZnO:Cu^{2+} samples were examined using the X-ray diffraction analysis in order to identify crystalline structure properties, and possible foreign phases. The main crystalline structure of all synthesized samples was in the hexagonal wurtzite phase (JCPDS No.36-1451), thus, all expectable Bragg planes was indexed in Fig. 1a.

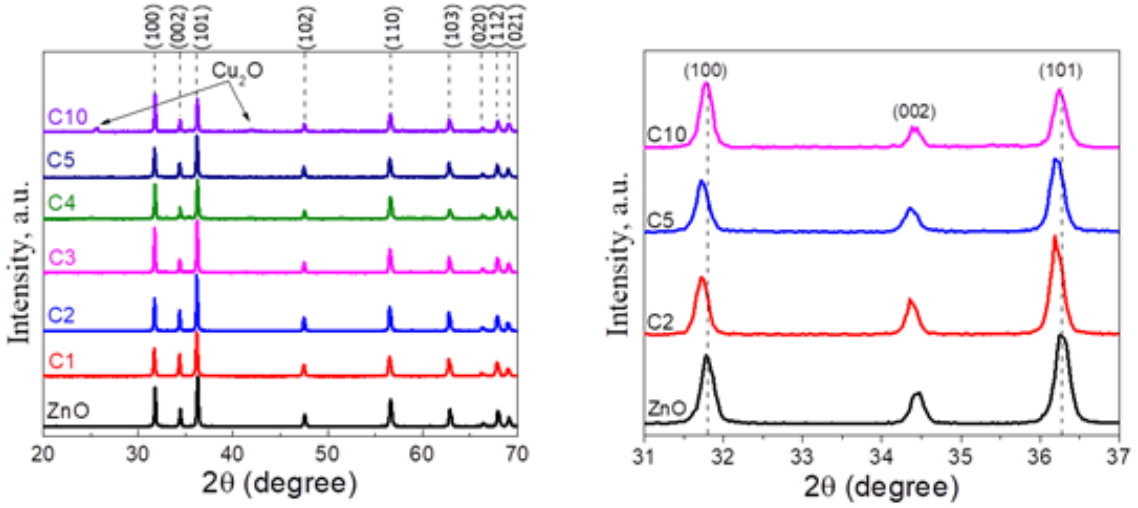

Fig. 1. a) X-ray diffraction patterns of ZnO with various Cu^{2+} content, b) Peaks were blue-shifted in doped samples.

The absence of extra peaks of the secondary phase in the diffraction patterns of ZnO and C1 - C5 implied that the produced powders obtained in the present work are in the pure wurtzite phase. When the dopant content increased, *i.e.* in samples with Cu^{2+} content larger than 5 at.%, the diffraction pattern of a foreign phase was observed at about 25.59˚, 35.37˚, and 41.91˚ which was belong to cuprite (Cu_2O), corresponding to [110], [111], and [200] directions, respectively (JCPDS No.05-0667) [19].

In order to see the effect of ion Cu^{2+} on crystalline deformation in the ZnO structure, the XRD patterns of ZnO, C2, C5 and C10 samples were extracted from 31^o to 37^o, as shown in *Fig. 1b*. Small blue-shifts of the main diffraction peaks confirmed the incorporation of Cu^+ in the ZnO lattice which increased the d-spacing value. This physical phenomenon was indicated that the dopant ion was successfully substituted Zn^{2+} in the ZnO host lattice and the transition metal ion should have a larger ionic radius than that of Zn^{2+} (0.074 nm). Since ionic radii of Cu^+ and Cu^{2+} are 0.096 and 0.073 nm, respectively, there is a transformation of the doubly charge Cu^{2+} from the precursor $Cu(NO_3)_2$ to the singly charge Cu^+ which is in agreement to the XRD result revealing the Cu_2O formation.

III.2. Scanning electron microscopy (SEM) analysis

Direct measurement of morphological features of prepared nanostructures was performed through the SEM analysis. Real space SEM images of undoped and doped ZnO nanostructures

were shown in *Fig. 2* and *Fig. 3*. A glimpse of SEM images vividly indicates the transformation of ZnO nanostructures through the Cu^{2+} ion doping concentration.

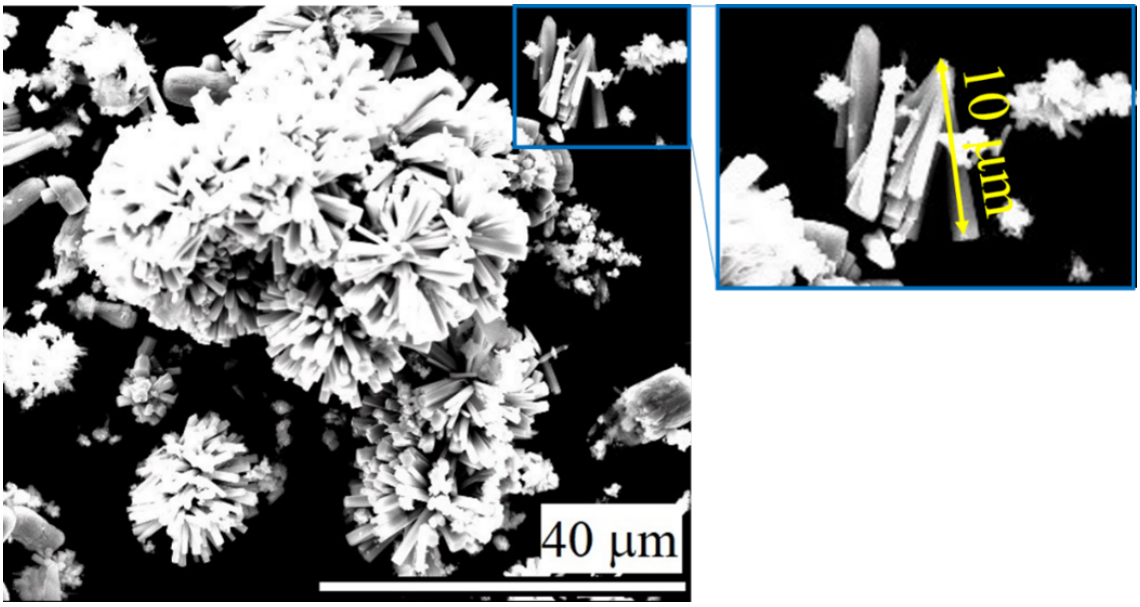

Fig. 2. Scanning electron microscopy images of the pure ZnO.

Figure 2 showed that the morphology of pure ZnO microstructure was flower-like and each flower had a homogeneous uniform rod-like distribution with a dimension of approximately 10 m in length, and 1.0-1.5 m in diameter. The hexagonal ZnO has a considerable degree of polarity in [0001] direction. Thus the *c*-axis (0001) of ZnO has a pronounced polar character. Terminated zinc, Zn- (0001), or terminated oxygen, O-(0001), in the [0001] direction could be in positively or negatively charged, respectively. Because charge of the each terminated surface is highly imbalanced, the moment of net dipole and the electrostatic potential will be considerably large and then the divergence of surface energy for large polar surfaces is produced. In hexagonal ZnO, the (0001) plane has a high instability and no surface reconstruction then ZnO prefers growing along this direction (*c*-axis) and termination with high polar surfaces of Zn^{2+}/O^{2+} interaction [8, 20]. When growing the crystalline structure, the precursor chemicals tend to adsorb onto this polar surfaces due to the high surface charge density to produce a high aspect ratio value. The alternativity of the polar surfaces is formed after a new positive/negative atomic layer is adsorbed, i.e. the O-terminated surface would be transformed into Zn-terminated surface, or vice versa [21]. The repeat of this adsorption continues during the ZnO crystallization process, then the [0001] direction will be the fastest rate of growth [22]. However, when *in situ* doping Cu^{2+} into ZnO, several effects would contribute to the variation of the polar surface energies which possibly induce the change in morphology.

Figure 3 showed the SEM images of synthesized Cu-doped ZnO samples. In general, the morphologies were changed by varying the dopant concentration. They were transferred from homogenous to imhomogenous cylinder size depending on the dopant content. With low starting

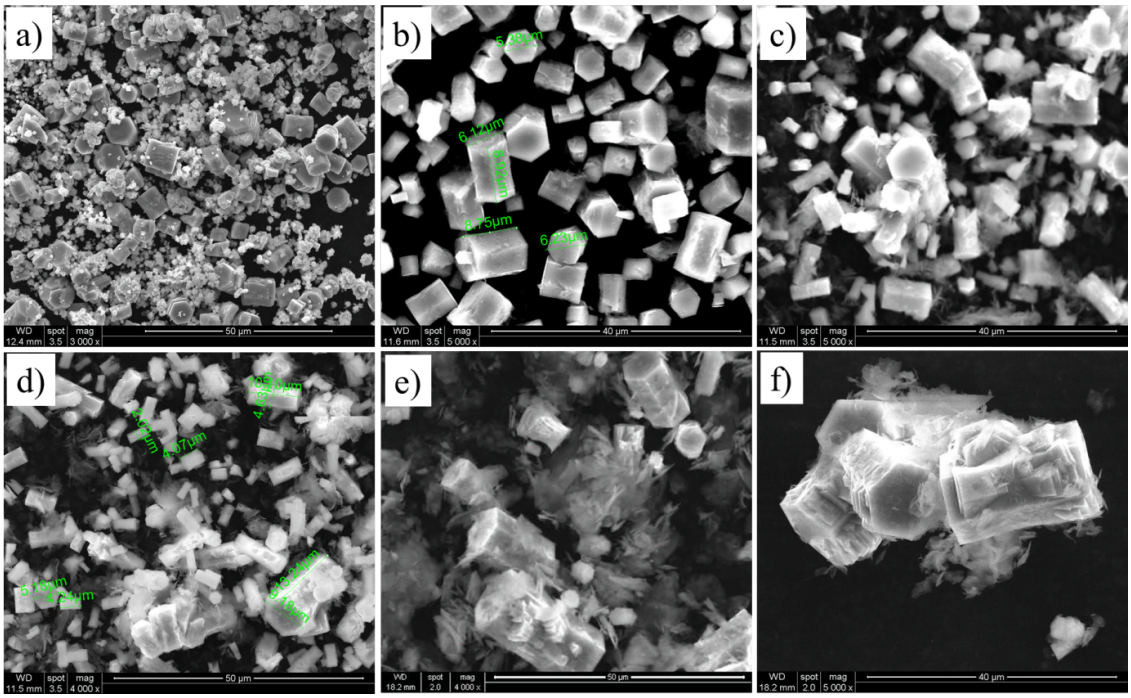

Fig. 3. Scanning electron microscopy images of the doped samples a) C1, b) C2, c) C3, d) C4, e) C5, and f) C10.

Cu^{2+} precursor contents, the aspect ratio (length/diameter) of ZnO shape was about 1.2, *i.e.*, for C1 and C2 samples. When dopant concentration was increased, the aspect ratio was increased, as for C3 and C4 samples. With the highest dopant concentration, the prism-like shape increased and the aspect ratio decreased. In more details, in *Fig. 3a*, besides the hexagonal rods with length of 5.5-7.4 m and diameter of 6.7-9.7 m, there was another structure as undeveloped nanoparticles. In this case, Cu-doped led to anisotropic growth not only caused the formation of the hexagonal rods but here onwards began to initialize the hexagonal prismatic shape. As comparing to flower-like shape in the pure ZnO, the rod was completely separated and dramatically decreased in the aspect ratio as a 1:1 prismatic cylinder. When the concentration of Cu^{2+} was increased, C2, as shown in *Fig. 3b*, the formation of the cylindrical prism was completed, thus there was no second phase of undeveloped particles. The formation of micro-cylindrical prism-like shape in C2 has the aspect ratio about 1.37 ± 0.2 which was larger than C1, 1.22 ± 0.2.

Considering the growth pattern of ZnO:Cu^{2+} nanostructures, we assumed that the developments of an anisotropy along the direction of *c*-axis, which was induced by the dopant Cu^{2+}, resulted in a variation from the flower-like shape in the pure ZnO to the cylindrical prism-like shape in C1, and C2. In the presence of Cu $^{2+}$, the charge on the Zn-terminated surface is less positive then the (0001) plane will reduce the polarization and the surface energy, thus weakening crystal growth on the *c*-axis. This along with the ionic radius of Cu^{+} greater than that of ion Zn^{2+} leads the reduction of the grown priority in this direction by the mismatch induced lattice strain. When the Cu^{2+} starting concentration increased to 3 and 4 at.%, the aspect ratio was increased and

the length distribution was broadly varied from 1.5 to 7.5 m. As shown in *Fig. 3c*, and Fig. 3d, the *c*-axis crystal growth was weakly maintained, thus stimulated the rupture of the cylinder prism. As one can see, these samples started to have the amorphous-like residual on the cylinder surfaces. At the highest Cu ion contents, C5 and C10, Fig. 3d and Fig. 3e showed a certain surface distortion by amorphous-like residual which remained in samples only large cylinders. The diameter size of the cylinder in C10 was around 15 m. As showed in the XRD pattern, the residual was cuprite (Cu_2O).

III.3. Mirco-Raman spectra

Raman vibration spectra study could support more information of structure disorder and dopant in crystalline materials. Moreover, this nondestructive method is a superior technique to detect dopant incorporation in the host lattice. Figure 4 shows the micro Raman spectra of ZnO, C2, and C5 samples. In general, when the dopant concentration increased, the Raman vibration modes of ZnO were sharper, and more intense which were different to a report of Fe ion doped ZnO micro-rod [13]. The most intensive mode in the Raman spectrum of pure ZnO is E_2^{high} at $\sim$435 cm^{-1} ascribed to oxygen vibration in the wurtzite phase [23]. When Cu^{2+} ions were introduced, the E_2^{high} signal was increased and blue-shifted to 437 and 439 cm^{-1} in the C2 and C5, respectively, followed by the narrowing. It is worthy to note that the E_2^{low} and E_2^{high} are assigned to non-polar active modes for Zn and O vibrations, respectively, whose intensities were increased in doped samples. In addition, with increase of the Cu^{2+} concentration, other ZnO characteristic modes in the Raman spectrum such as $A_1(TO)$, $E_1(TO)$ and $E_1(LO)$ were also observed at around 382, 415 and 582 cm^{-1}, respectively. Moreover, according to the Raman spectra of C2 and C5 there was a signal at $\sim$628 cm^{-1} assigned to Cu_2O [24]. In the C5 sample, there subtle signals appeared in a range of 640-660 cm^{-1} also were assigned to $\Gamma_{15}^{-1}(LO)$ and $\Gamma_{15}^{-1}(TO)$ vibrations of Cu_2O [25].

III.4. Models for (0001) plane growth mechanism studied by polar surface reconstruction

The stability of singly positive ion Cu^+ oxidation state: ZnO is an unintentional n-type semiconductor which has a high electron density in the conduction band region. When doped with Cu^{2+}, electron configuration $[Ar]3d^9$, ion Cu^{2+} will play as an electron trap center that will trap a conduction band electron [10] as shown in Fig. 5, *i.e.* $Cu^{2+} + e^- \rightarrow Cu^+$. Moreover, the XRD pattern of C10 revealed the Cu_2O phase indicated the higher stability of the oxidation state for Cu^+ in comparison to Cu^{2+}. Hence the excess electrons in the ZnO conduction band were readily transferred to form a completely filled 3d-shell of Cu^+ ion. It is worthy to note that the alkaline environment, due to the HMTA precursor as a weak base, also contributed to this reduction process [26]. The substituted Cu^+ site causes Zn-terminated (0001) surface being less positive charge density, in the view of electrostatic consideration, the polar surface energy, and then alternative distances are increased along the $[0001]$ direction. As a consequence, the *c*-axis growth is less favorable.

Reconstruction of polar surface energy: As mentioned above, the formation of bonding in the ZnO is from electrostatic force and the polar surface along the c-axis can be positive (Zn-terminated) or negative (O-terminated). In addition, it was reported that the Zn-terminated (0001) surface is

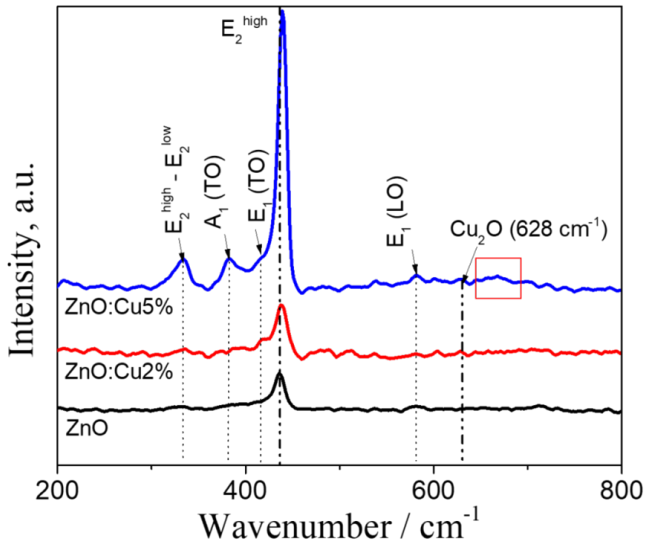

Fig. 4. Raman spectra of as-prepared ZnO and Cu-doped ZnO.

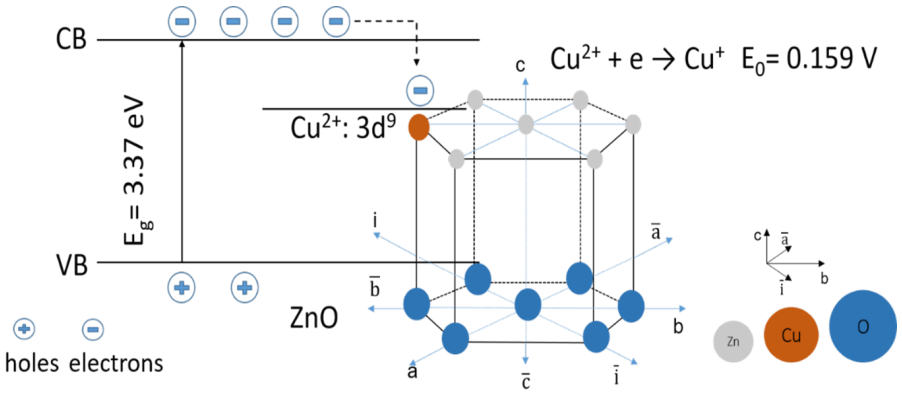

Fig. 5. Mechanism model for electron migration.

chemically active, and the O-terminated $(000\bar{1})$] surface is chemically inert [18, 27]. Morphological evolution could be comprehended on the basis of polarized surface energy and crystal deformation due to the diffusion of Cu^{+} ions. The crystal growth mechanism of the microstructure can be appropriately explained based on the schematic diagram in Fig. 6.

The substitution of Zn^{2+} ions by Cu^{+} ions initiates with 1 at.% Cu and 2 at.% Cu are shown in Fig. 6b. The crystallographic anisotropy with the high imbalance will prefer the anisotropic growth. During ZnO crystal growth, the Cu ions tend to adsorb onto Zn-terminated (0001) polar surfaces. Because of the difference in charge and ionic radii, when singly positive charge Cu^{+}ions

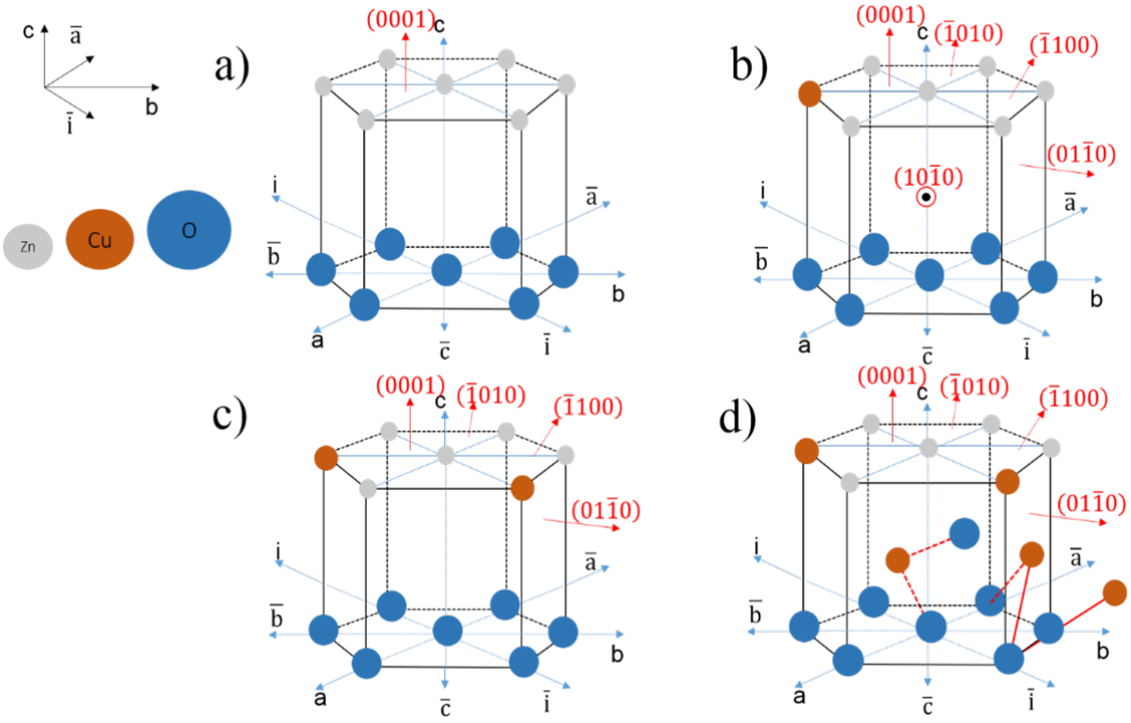

Fig. 6. The schematic depicting dopant concentration driven the development orientation of the microstructures: a) ions arrangement for undoped ZnO, b) proposed for C1, C2, c) proposed for C3, C4, and d) proposed for C5, C10.

substitutionally replace Zn^{2+}, the surface electrostatic potential decreases and lattice distortion is intensified. When the content of dopant is increased, the mismatch of ZnO crystal induces stress and strain that consequently effect on the normal growth. For example, based on *Fig. 6b* and *Fig. 6c*, the crystals begin to develop in other directions such as: $(10\bar{1}0)$, $(01\bar{1}0)$, $(\bar{1}100)$, $(\bar{1}010)$, in C1, C2 samples and $(01\bar{1}0)$, $(\bar{1}100)$, $(\bar{1}010)$, in C3, C4 samples, hence the (0001) plane has no longer the dominant priority for growing. As a result, the rod length becomes shorter and the diameter is larger, i.e. smaller in aspect ratio value. This is resulted in the transformation of microrods into hexagonal prisms for 2 at.% Cu^{2+} doped ZnO (Fig. 6c). Thus, formation of hexagonal cylinder is an evidence of reducing anisotropic growth along c-axis where Cu ions preferably accumulate on chemically active $[(0001)] - Zn$ top surface. With increased Cu doping (*i.e.*, for C3, and C4), the rod size varies broadly indicating the difficulty of the growth along the $[0001]$ direction. The active Zn-terminated polar surface becomes more stable and hence, instead of the (0001) plane anisotropic growth, now the crystalline growth initiates in other planes and gets prominent afterwards with increasing the Cu^{2+} content. With the highest dopant contents in C5 and C10, the small rods were disappeared and growing process preferred to produce larger rods. In a nutshell, substitutional Cu^{+} ions reduced the polarization on the (0001) plane which has a large impact on the anisotropy development of ZnO.

IV. CONCLUSIONS

This work presented a facile hydrothermal method to fabricate ZnO micro-rods doped with various contents of Cu^{2+} ion. The phase and morphology depended on the dopant content were systematically investigated by XRD, Raman vibration and SEM. The undoped ZnO was formed in the flower-like shape with a high anisotropy micro-rod with $\sim$1.5 m in diameter and $\sim$10 m in length. When *in situ* introducing Cu $^{2+}$ ion into the ZnO lattice, the anisotropy characteristic of [0001] direction was dramatically reduced to form ZnO as a hexagonal prism-like shape which was larger in diameter and smaller in the aspect ratio. The mechanism of the growing process was proposed in a view of polar surface energy reconstruction and the electron trap character of Cu^{2+} centre. It suggested the electron migration from ZnO conduction band to unfilled d-state shell of the ion Cu^{2+}, *i.e.* $Cu^{2+} + e^- \rightarrow Cu^+$. Hence, Zn-terminated surface is less positive which could attribute to the reduction of the growing process along the [0001] direction.

ACKNOWLEDGMENT

This research is funded by Vietnam National Foundation for Science and Technology Development (NAFOSTED) under grant number 103.02-2019.362.

REFERENCES

[1] M. Scarrozza, G. Pourtois, M. Houssa, M. Caymax, A. Stesmans, M. Meuris and M. M. Heyns, *A theoretical study of the initial oxidation of the GaAs(001)-?2(24) surface*, *Appl. Phys. Lett.* **95** (2009) 253504.

[2] C. Noguera, *Polar oxide surfaces*, *J. Phys. Condens. Matter* **12** (2000) R367.

[3] D. Mora-Fonz, T. Lazauskas, M. R. Farrow, C. R. A. Catlow, S. M. Woodley and A. A. Sokol, *Why are polar surfaces of ZnO stable?*, *Chem. Mater.* **29** (2017) 5306.

[4] C. T. Quy, N. X. Thai, N. D. Hoa, D. T. Thanh Le, C. M. Hung, N. Van Duy and N. Van Hieu, *C_2H_5OH and NO_2 sensing properties of ZnO nanostructures: correlation between crystal size, defect level and sensing performance*, *RSC Adv.* **8** (2018) 5629.

[5] M. Tonezzer, T. T. L. Dang, N. Bazzanella, V. H. Nguyen and S. Iannotta, *Comparative gas-sensing performance of 1D and 2D ZnO nanostructures*, *Sensor Actua. B Chem.* **220** (2015) 1152.

[6] G. H. Mhlongo, K. Shingange, Z. P. Tshabalala, B. P. Dhonge, F. A. Mahmoud, B. W. Mwakikunga, D. E. Motaung, *Room temperature ferromagnetism and gas sensing in ZnO nanostructures: Influence of intrinsic defects and Mn, Co, Cu doping*, *Appl. Surf. Sci.* **390** (2016) 804.

[7] Y. Xia, P. Yang, Y. Sun, Y. Wu, B. Mayers, B. Gates, Y. Yin, F. Kim and H. Yan, *One-dimensional nanostructures: synthesis, characterization, and applications*, *Adv. Mater.* **15** (2003) 353.

[8] J.Miao and B.Liu, *II-VI Semiconductor nanowires: ZnO, Semiconductor Nanowires: Materials, Synthesis, Characterization and Applications*, Elsevier Ltd., 2015.

[9] I. Žutić, J. Fabian and S. Das Sarma, *Rev. Mod. Phys.* **76** (2004) 323.

[10] S. Choi, J. Y. Do, J. H. Lee, C. S. Ra, S. K. Kim and M. Kang, *Optical properties of Cu-incorporated ZnO (Cu x Zn y O) nanoparticles and their photocatalytic hydrogen production performances*, *Mater. Chem. Phys.* **205** (2018) 206.

[11] A. Meng, J. Xing, Z. Li and Q. Li, *Cr-Doped ZnO nanoparticles: synthesis, characterization, adsorption property, and recyclability*, *ACS Appl. Mater. Interfaces* **7** (2015) 27449.

[12] N. A. Putri, V. Fauzia, S. Iwan, L. Roza, A. A. Umar and S. Budi, *Mn-doping-induced photocatalytic activity enhancement of ZnO nanorods prepared on glass substrates*, *Appl. Surf. Sci.* **439** (2018) 285.

[13] A. Sahai, Y. Kumar, V. Agarwal, S.F. Olive-Mndez, N. Goswami, *Doping concentration driven morphological evolution of Fe doped ZnO nanostructures*, *J. Appl. Phys.* **116** (2014) 164315.

[14] A. N. Kadam, T. G. Kim, D. S. Shin, K. M. Garadkar and J. Park, *Morphological evolution of Cu doped ZnO for enhancement of photocatalytic activity*, *J. Alloys Compd.* **710** (2017) 102.

[15] M. Babikier, D. Wang, J. Wang, Q. Li, J. Sun, Y. Yan, Q. Yu and S. Jiao, *Cu-doped ZnO nanorod arrays: the effects of copper precursor and concentration*, *Nanoscale Res. Lett.* **9** (2014) 199.

[16] O. Dulub, U. Diebold and G. Kresse, *Novel stabilization mechanism on polar surfaces: ZnO(0001)-Zn*, *Phys. Rev. Lett.* **90** (2003) 016102.

[17] J. V. Lauritsen, S. Porsgaard, M. K. Rasmussen, M. C. Jensen, R. Bechstein, K. Meinander, B. S. Clausen, S. Helveg, R. Wahl, G. Kresse and F. Besenbacher, *Stabilization principles for polar surfaces of ZnO*, *ACS Nano* **5** (2011) 5987.

[18] V. Staemmler, K. Fink, B. Meyer, D. Marx, M. Kunat, S. Gil Girol, U. Burghaus and C. Woll, *Stabilization of polar ZnO surfaces: validating microscopic models by using CO as a probe molecule*, *Phys. Rev. Lett.* **90** (2003) 106102.

[19] Y. Yang, D. Xu, Q. Wu and P. Diao, *Cu_2O/CuO bilayered composite as a high-efficiency photocathode for photoelectrochemical hydrogen evolution reaction*, *Sci. Rep.* **6** (2016) 35158.

[20] C. Ye, X. Fang, Y. Hao, X. Teng and L. Zhang, *Zinc oxide nanostructures: morphology derivation and evolution*, *J. Phys. Chem. B* **109** (2005) 19758-19765.

[21] S. Xu and Z. L. Wang, *One-dimensional ZnO nanostructures: Solution growth and functional properties*, *Nano Res.* **4** (2011) 1013.

[22] Z. L. Wang, *Zinc oxide nanostructures: growth, properties and applications*, *J. Phys. Condens. Matter* **16** (2004) R829.

[23] N. Goswami and A. Sahai, *Structural transformation in nickel doped zinc oxide nanostructures*, *Mater. Res. Bull.* **48** (2013) 346.

[24] Y. Deng, A. D. Handoko, Y. Du, S. Xi and B. S. Yeo, *In Situ Raman spectroscopy of copper and copper oxide surfaces during electrochemical oxygen evolution reaction: identification of CuIII oxides as catalytically active species*, *ACS Catal.* **6** (2016) 2473.

[25] M. Ivanda, D. Waasmaier, A. Endriss, J. Ihringer, A. Kirfel and W. Kiefer, *Low-temperature anomalies of cuprite observed by Raman spectroscopy and x-ray powder diffraction*, *J. Raman Spectrosc.* **28** (1997) 487.

[26] M. A. Rizvi, S. A. Akhoon, S. R. Maqsood and G. M. Peerzada, *Synergistic effect of perchlorate ions and acetonitrile medium explored for extension in copper redoximetry*, *J. Anal. Chem.* **70** (2015) 633.

[27] Z. L. Wang, X. Y. Kong and J. M. Zuo, *Induced growth of asymmetric nanocantilever arrays on polar surfaces*, *Phys. Rev. Lett.* **91** (2003) 185502.